Decolorization of organic dyes on Pilkington Activ™ photocatalytic glass

Paul Chin, David F. Ollis *

Department of Chemical and Biomolecular Engineering, Box 7905, North Carolina State University, Raleigh, NC 27695-7905, USA

Available online 23 March 2007

Abstract

The air–solid photocatalytic degradation of organic dye films Acid Blue 9 (AB9) and Reactive Black 5 (RBk5) is studied on Pilkington Activ™ glass. The Activ™ glass comprises of a colorless TiO_2 layer deposited on clear glass. The Activ™ glass is characterized using atomic force microscopy (AFM) and X-ray diffraction (XRD). Using AFM, the TiO_2 average agglomerate particle size is 95 nm, with an apparent TiO_2 thickness of 12 nm. The XRD results indicate the anatase phase of TiO_2, with a calculated crystallite size of 18 nm.

Dyes AB9 and RBk5 are deposited in a liquid film and dried on the Activ™ glass to test for photodecolorization in air, using eight UVA blacklight-blue fluorescent lamps with an average UVA irradiance of $1.4 \ mW/cm^2$. A novel horizontal coat method is used for dye deposition, minimizing the amount of solution used while forming a fairly uniform dye layer. About 35–75 monolayers of dye are placed on the Activ™ glass, with a covered area of $7–10 \ cm^2$. Dye degradation is observed visually and via UV–vis spectroscopy.

The kinetics of photodecolorization satisfactorily fit a two-step series reaction model, indicating that the dye degrades to a single colored intermediate compound before reaching its final colorless product(s). Each reaction step follows a simple irreversible first-order reaction rate form. The average k_1 is 0.017 and $0.021 \ min^{-1}$ for AB9 and RBk5, respectively, and the corresponding average k_2 is 2.0×10^{-3} and $1.5 \times 10^{-3} \ min^{-1}$. Variable light intensity experiments reveal a $p = 0.44 \pm 0.02$ exponent dependency of initial decolorization rate on the UV irradiance. Solar experiments are conducted outdoors with an average temperature, water vapor density, and UVA irradiance of 30.8 °C, 6.4 g water/m^3 dry air, and $1.5 \ mW/cm^2$, respectively. For AB9, the average solar k_1 is $0.041 \ min^{-1}$ and k_2 is $5.7 \times 10^{-3} \ min^{-1}$.

1. Introduction

Technological advances in the past decade allow glass manufacturers to deposit thin photoactive TiO_2 layers on glass, with trademark names such as Activ™ [1], Sunclean™ [2], and Bioclean™ [3]. These products are billed as "self-cleaning" surfaces because they utilize TiO_2 photocatalytic oxidation (PCO) and photo-induced superhydrophilicity (PSH) properties. The PCO activity causes progressive oxidation of adsorbed oxidizable molecules and particulate matter, while the PSH property allows for water washing removal of partially oxidized molecules and particulates from the photocatalytic surface.
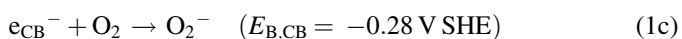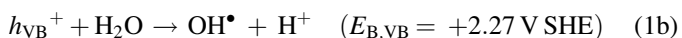
The PCO property of self-cleaning glass is activated by absorption of UV light of energy higher than the TiO_2 band gap energy (E_{BG}). Electron photoexcitation from the TiO_2 valence band (VB) to the conduction band (CB) produces electron

(e_{CB}^-)–hole (h_{VB}^+) pairs (Eq. (1a)). For anatase phase TiO_2, $E_{BG} = 3.2$ eV ($\lambda = 385$ nm), while rutile phase TiO_2 has a $E_{BG} = 3.0$ eV ($\lambda = 410$ nm). The redox potential for h_{VB}^+ is +2.53 V with respect to the standard hydrogen electrode (SHE), which is enough energy to overcome the +2.27 V SHE binding energy to form $OH^\bullet$ ($E_{B,VB}$) [4], shown in Eq. (1b). Similarly, e_{CB}^- (−0.52 V SHE redox potential) can react with O_2 to form O_2^- ($E_{B,CB} = -0.28$ V SHE) [4], shown in Eq. (1c). The O_2^- may combine with H^+ to form $O_2H^\bullet$ (Eq. (1d)). These oxygen containing radicals are responsible for adsorbate oxidation to volatile and/or water soluble products, generating the "self-cleaning" effect. The full reaction sequence for TiO_2 photocatalysis is detailed elsewhere [5]. Similar to the PCO property, the PSH mechanism of TiO_2 is activated by UV light. Two mechanisms have been proposed elsewhere [4,6] to describe the ability of TiO_2 to change from a hydrophobic to a hydrophilic surface after UV illumination.

$$TiO_2 \overset{h\nu \geq E_{BG}}{\longrightarrow} e_{CB}^- + h_{VB}^+ \quad (E_{BG} = 3.0 - 3.2 \, \text{eV}) \quad (1a)$$

* Corresponding author. Tel.: +1 919 515 2329; fax: +1 919 515 3465.
  E-mail address: ollis@ncsu.edu (D.F. Ollis).

$$h_{VB}{}^+ + H_2O \rightarrow OH^\bullet + H^+ \quad (E_{B,VB} = +2.27 \text{ V SHE}) \quad (1b)$$

$$e_{CB}{}^- + O_2 \rightarrow O_2{}^- \quad (E_{B,CB} = -0.28 \text{ V SHE}) \quad (1c)$$

$$O_2{}^- + H^+ \rightarrow O_2H^\bullet \quad (1d)$$

We continue here our exploration of photocatalyzed dye degradation in air–solid systems because of its potential as a field analysis method to characterize initial and continuing photocatalytic activity of installed ''self-cleaning'' window glass. Research to date on organic dye degradation by TiO_2 has focused on aqueous–solid systems, since dye wastewater treatment is a current environmental challenge. There have been few papers [7–9] on air–solid dye systems. Vinodgopal et al. [7] studied dye photosensitization of Acid Orange 7 (AO7) on Degussa P25 TiO_2 in an air–solid system. Diffuse reflectance laser flash photolysis experiments at sub-bandgap wavelengths ($\lambda = 532$ nm) yielded dye degradation of samples exposed to air, but negligible degradation of degassed samples. Yang et al. [8] oxidized Acid Blue 9 (AB9) on nano-sized TiO_2 in aqueous and air–solid systems. Their aqueous results were fit to a first-order kinetic model, but they did not propose a kinetic model for their air–solid data. Julson and Ollis [9,10] researched decolorization in air of dyes Reactive Blue 19, Reactive Black 5 (RBk5), AB9, and AO7 on Degussa P25 TiO_2 and alumina (Alu C Al_2O_3) powders. Minimal homogeneous photo-degradation on Al_2O_3 was reported, but on TiO_2, the PCO decolorization data was fit to a two step series reaction model, described in detail later.

Thin films of TiO_2 [11–21] have been coated on a variety of surfaces for air and water remediation. Doushita and Kawahara [12] coated glass substrates with a TiO_2 sol–gel solution using the spin coat method and fired the substrate to 318 °C to give TiO_2 an anatase structure. They mixed methylene blue and AB9 with polyvinyl alcohol binder, water, and ethanol, and then deposited the solution on the TiO_2 thin films. Binder degradation was negligible for UV illumination times less than 10 min, but the radical species such as $OH^\bullet$ and $O_2H^\bullet$ presumably diffused within the binder layer to react with the entrapped dyes. They proposed a diffusion–reaction model, but made no attempt to fit the model to their data.

Sitkiewitz and Heller [13] applied 0.3 ± 0.1 μm TiO_2 layers on glass slides by spin coating a sol–gel solution. Vapor phase benzene and condensed phase stearic acid were oxidized separately over 4 h test periods. In the presence of H_2O and O_2, the CO_2 generation rate for both pollutants was linear with a zero-order rate constant of 10^{-2} μmol CO_2/(h cm^2 TiO_2) for UV irradiances ($\lambda = 365$ nm) varying from 0.3 to 5.8 mW/cm^2, while minimal or no CO_2 was produced in the absence of O_2 or H_2O. The CO_2 generation rate was proportional to the square root of irradiance for UVA values ranging from ∼0.1 to 6.0 mW/cm^2.

Romeas et al. [14] sprayed ∼580 nm thick layers of palmitic acid, a C_{15} molecule, on glass plates dip-coated with TiO_2 and an unstated photostable binder. They observed zero-order kinetics with a rate constant of 0.60 ± 0.12 μmol/h of palmitic acid at 0.7–1 mW/cm^2 irradiance and 18–22 °C temperature

conditions. The zero-order kinetics was rationalized by constant saturation of the TiO_2 surface by palmitic acid, and a negligible diffusion resistance for O_2 supply. Identified intermediate products included C_8–C_{12} carboxylic acids on the glass plate, and various lower MW alkanes, alcohols, aldehydes, ketones, and C_1–C_{13} carboxylic acids in the vapor phase.

Pilkington Activ^{TM} ''self-cleaning'' glass has been investigated by Mills et al. [21] for oxidation of stearic acid films. For thick layers of stearic acid (61–75 monolayers), the initial kinetics were zero-order for disappearance of the integrated area of CH_2– and CH_3– group IR bands. In the absence of stearic acid, contact angle measurements on Activ^{TM} glass showed that 45 min of UV light exposure decreased the water contact angle from 67° (hydrophobic) to 0° (hydrophilic). Complete dark recovery of the water contact angle after UV illumination required 120–150 h. To date, only Mills et al. [21] have tested the commercial Activ^{TM} glass for stearic acid destruction.

Our present work further characterizes the PCO properties of Activ^{TM} glass using organic dyes (rather than stearic or palmitic acid) deposited in a liquid film, then dried on the Activ^{TM} glass, and subsequently oxidized (a) to show visual decolorization and recovery of the aesthetic clarity of the glass and (b) to determine the light-driven reaction kinetics on Activ^{TM} glass.

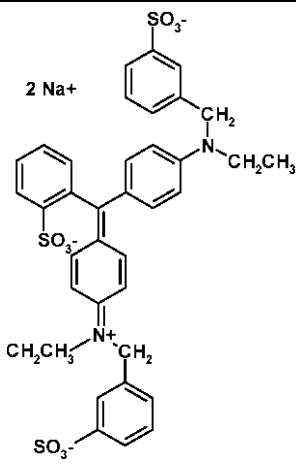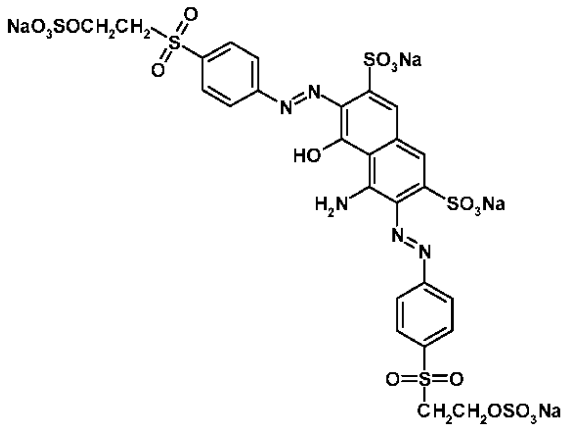## 2. Experimental

2.1. Materials

The dyes Brilliant Blue FCF (C.I. Acid Blue 9, or AB9) and Remazol Black B (C.I. Reactive Black 5, or RBk5) were purchased from Fisher Scientific and used as received. The composition, structure, and optical characteristics of AB9 and RBk5 are reported in Table 1. The 10 cm (l) × 10 cm (w) × 0.3 cm (h) Pilkington Activ^{TM} TiO_2-coated glass and the Pilkington Optifloat^{TM} clear glass (non-photocatalytic control reference) were gifts from Pilkington PLC and were cut into 10 cm (l) × 2.5 cm (w) × 0.3 cm (h) pieces. A Jelight Company Inc. Model #42 ultraviolet-ozone (UVO) cleaner was used to remove any initial organic contaminants on the glass surface. A KD Scientific KDS100 syringe pump with a linear motor ranging from 1 to 100 mL/h (2.12–212 μm/s) allowed dye solution deposition on the glass surfaces.

The laboratory photoreactor, described elsewhere [9], consisted of eight parallel General Electric 20W UVA black-light-blue fluorescent lamps (peak emission $\lambda = 365$ nm) mounted in a 66 cm (l) × 46 cm (w) × 71 cm (h) enclosed, painted wooden box. A small fan brought in fresh air and maintained ambient temperature conditions. The UVA light intensity (320–390 nm) was measured by a Control Company Traceable^{TM} UV Light Meter, and temperature and relative humidity (RH) measurements were obtained with a Traceable^{TM} Memory Hygrometer/Thermometer.

Dye decolorization was followed (a) photographically using a Canon Powershot S30 3.2 megapixel digital camera and (b) optically via absorbance data from a Jasco V-550 UV–Visible

Table 1
Characteristics of dyes Acid Blue 9 and Reactive Black 5

Dye	Chemical structure	M_W (g/mol)	Abs peaks (λ) (nm)	Molar absorptivity (α) (L/(mol cm))
Acid Blue 9 $C_{37}H_{34}N_2Na_2O_9S_3$ acid triphenylmethane dye, CAS No. 3844-45-9		792.9	629 408	86,600 8730
Reactive Black 5 $C_{26}H_{21}N_5Na_4O_{19}S_6$ reactive vinylsulphone disazo dye, CAS No. 17095-24-8		991.8	597 392	27,600 2830

spectrophotometer. The clean Activ™ glass surface was characterized by atomic force microscopy (AFM) and X-ray diffraction (XRD), as described below.

2.2. Characterization of Pilkington Activ™ glass

The average TiO_2 particle size and apparent thickness (height) were determined using a Digital Instruments Dimension™ 3000 AFM, with a NanoScope IIIa controller and a vibration-shielded hood. The AFM imaging was performed in contact and tapping modes. The tapping mode employed an OTESPA model Si cantilever from Veeco Probes with a 7 nm nominal tip radius and a 12–103 N/m spring constant. The contact mode employed a DNP-S20 model Si_3N_4 cantilever from Veeco Probes with a 10 nm nominal tip radius and 0.06–0.58 N/m spring constant. All measurements were done on 1 μm × 1 μm area under ambient conditions, with 256 samples per image and a scan rate of 1 Hz. In tapping mode, the drive frequency was 330 kHz. The surface root-mean-square roughness (R_q) and the maximum height (R_{max}) are defined as the standard deviation of the surface height (Z) and the largest Z difference within the image area, respectively.

Atomic spacing and crystallite size were determined using an Inel XRG 3000 X-ray diffractometer that employed Cu Kα_1 radiation (λ = 1.5405 Å). Data was collected using a CPS-120 detector over $0° < 2\theta < 69°$ angles. The data was calibrated with respect to a potassium alum standard. The characteristic *d*-spacing between atomic planes (*d*) is calculated from Bragg's law (Eq. (2)), where θ_B is the Bragg angle (° or rad) and λ is the radiation wavelength. The crystallite size (*x*) is obtained from the Scherrer equation (Eq. (3)), where *K* is the prefactor coefficient ranging from 0.9 to 1.0 (assumed to equal one) and β is the full width at half maximum. The Scherrer equation is derived for cubic crystal configuration, but it provides a good estimate for different geometries [22] (anatase and rutile: tetragonal; brookite: orthorhombic [23]). The effects of instrument broadening, microstrain, and faulting are ignored in Eq. (3):

$$\lambda = 2d \sin \theta_B \qquad (2)$$

$$x = \frac{K\lambda}{\beta \cos \theta_B} \qquad (3)$$

2.3. Deposition procedure

Two and 10 mM concentration solutions of AB9 and RBk5 in DI water were prepared. The Activ^{TM} glass was placed in the UVO cleaner for 10 min to remove surface contaminants and to make the surface hydrophilic. Then the dye solutions were deposited on the Activ^{TM} glass using a rapid convective assembly method developed by Prevo and Velev [24]. Their novel horizontal, moving "dip coat" method formed a fairly uniform dye layer and minimized the quantity of dye solution used. The dye coverage on the glass could be controlled by adjusting the dye concentration, motor speed, or injection volume.

For our experiments, a 15 μL injection volume of 2 or 10 mM AB9 or RBk5 in DI water was placed between the Activ^{TM} glass and the deposition slide. The deposition slide was fitted with a Teflon spacer to reduce scraping of the TiO$_2$ thin film. The linear motor spread the dye injection volume across the slide at a velocity of 10.6 μm/s (5 mL/h) at ambient lab air conditions ($T = 21$–24 °C; RH = 20–50%) unless noted otherwise. The terms "thin" and "thick" multilayers describe the deposition of 2 and 10 mM dye solutions, respectively, corresponding to 40–75 and 150–260 layers of dye on the subsequent dried surface. Control experiments were run on the Optifloat^{TM} glass following the same dye deposition procedure used for the Activ^{TM} glass.

2.4. Testing conditions

The dried, dye-coated Activ^{TM} and Optifloat^{TM} glass samples were placed in the laboratory photoreactor, where typical experiments were run at a UVA light intensity of 1.4 mW/cm^2 achieved by placing the glass samples 24 cm below the lamps. Experiments were stopped at given time intervals, and absorbance data was collected from 390 to 800 nm using the UV–vis spectrophotometer. The spectra scan stopped at 390 nm to prevent photocatalyzed reaction propagation by TiO$_2$. Light intensity-influenced experiments on the Activ^{TM} glass were conducted in the laboratory photoreactor. Light intensity was varied by adjusting the distance of the Activ^{TM} glass samples from the lamps. The three resulting light intensities were 1.8–1.9, 0.70–0.77, and 0.08–0.10 mW/cm^2. In all indoor photoreactor experiments, the measured lab air temperature was 22 ± 2 °C and the water vapor density was 7 ± 2 g/m^3 dry air (approximately 25–50% relative humidity).

Solar experiments on the Activ^{TM} glass were run outdoors at midday (1000–1700 h) for up to 3 days on the top floor of a parking deck in Raleigh, North Carolina. The uncontrolled UVA light intensity varied from 0.30 to 2.05 mW/cm^2 under sunny and cloudy spring conditions. The average outside temperature was 31 °C, with a standard deviation of 4 °C and a minimum and maximum of 20 and 39 °C, respectively. The average vapor density was 7 g water/m^3 dry air (22% relative humidity), with a standard deviation of 3 g/m^3 and a minimum and maximum of 2 and 11 g/m^3, respectively (approximately 6–35% relative humidity).

2.5. Data analysis

Dye decolorization was observed visually, and digital photographs were taken at various time intervals. UV–vis absorbance data was collected and related to dye concentration using the Beer–Lambert law (Eq. (4)), where Abs is the absorbance, α the molar absorptivity at wavelength λ (L/(mol cm) or cm^2/mol) of each colored compound (i.e., dye and intermediate), b the path length (cm), C the colored compound solution concentration (mol/L), and C_{app} is the colored compound molar value per unit glass surface area covered by the compound (mol/cm^2):

$$\text{Abs} = \alpha b C = \alpha C_{app} \qquad (4)$$

3. Results and discussion

3.1. Atomic force microscopy

Fig. 1 shows AFM images of the Activ^{TM} and Optifloat^{TM} glass. The R_q values for the Activ^{TM} and Optifloat^{TM} glass were 2.3 and 0.4 nm, respectively. The R_{max} for the Activ^{TM} glass was 21.1 nm versus only 4.5 nm for the Optifloat^{TM} glass. These results indicate greater roughness on the Activ^{TM} glass, and verify a coated layer on the Activ^{TM} surface compared to the smoother Optifloat^{TM} clear glass. According to Mills et al. [21], their SEM images showed broad TiO$_2$ domes of about 30 nm diameter on Activ^{TM}. From the top-down view in Fig. 1a, our average TiO$_2$ particle diameter is 95 nm with a standard deviation of 30 nm. Our TiO$_2$ diameter was calculated from 30 random measurements of the broad dome shapes. Our measured particle diameter is 3× larger than Mills' value, but this difference may be caused by overlapping TiO$_2$ peaks that cannot be resolved from the top-down view. Overlapping TiO$_2$ hemispherical peaks are seen in the topographical view (Fig. 1b) and the sectional view (not shown).

From the sectional AFM view (not shown) averaged over seven measurements, the TiO$_2$ thickness is 12 nm. This value is similar to those reported by Mills et al. [21] (15 nm) and the Sanderson and Knowles patent [25] (10–20 nm).

3.2. X-ray diffraction

Fig. 2 shows the smoothed XRD results from the Activ^{TM} glass, with the Optifloat^{TM} clear glass results subtracted as a baseline. There is considerable noise, but a clear peak at 25.15° corresponds to a d-spacing of 3.54 Å using Bragg's law (Eq. (2)). Anatase phase TiO$_2$ has its highest intensity at the (1 0 1) plane with $d = 3.52$ Å ($2\theta_B = 25.28°$ for Cu Kα_1 radiation) [26]. Brookite phase TiO$_2$ also has its highest intensity at $d = 3.51$ Å ($2\theta_B = 25.35°$ for Cu Kα_1 radiation) [26]. Since no other peaks are seen for brookite phase TiO$_2$
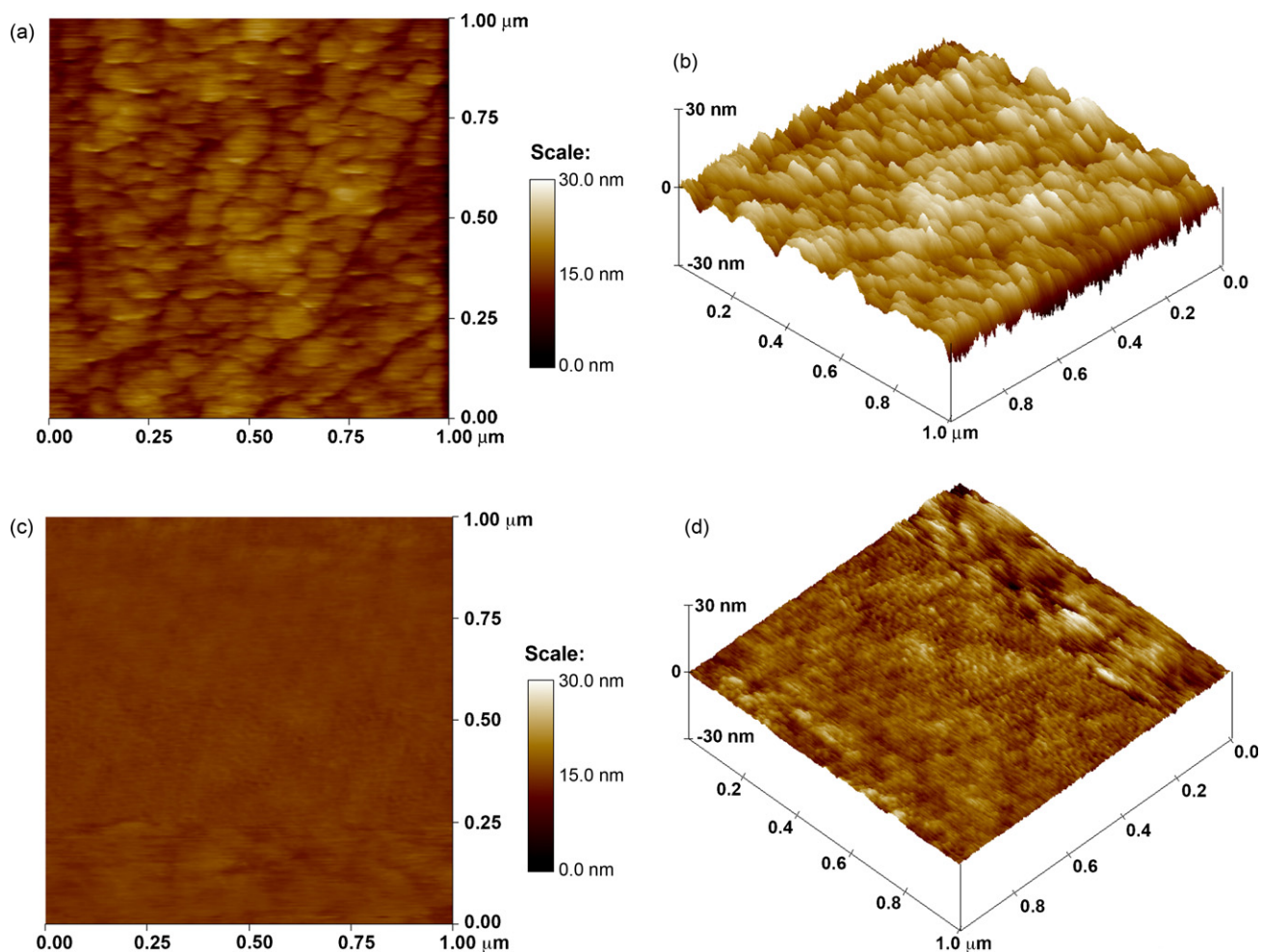
Fig. 1. AFM images of 3 mm Pilkington Activ[TM] glass in (a) a top-down view and (b) a topographical view, and 3 mm Pilkington Optifloat[TM] clear glass in (c) a top-down view and (d) a topographical view.

(90% and 80% maximum intensities at $d = 2.90$ and 3.47 Å, respectively), we conclude that TiO_2 is in the anatase phase. No peaks are seen associated with rutile phase TiO_2. We use the Scherrer equation (Eq. (3)) to approximate the TiO_2 crystallite
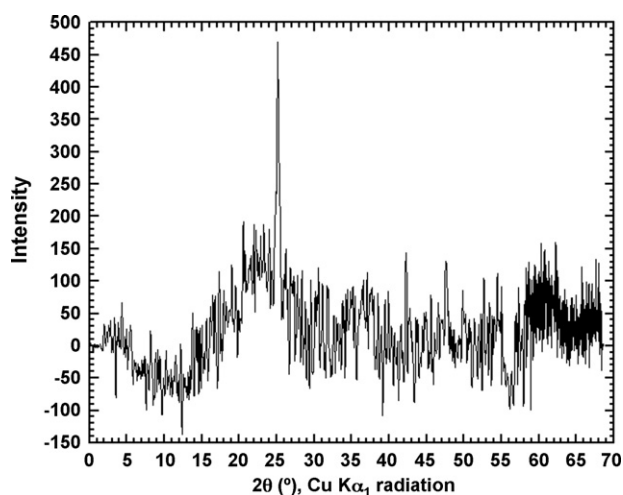

Fig. 2. Smoothed XRD image of 3 mm Pilkington Activ[TM] glass. A peak at $2\theta = 25.15°$ corresponds to anatase phase TiO_2.

thickness. From Fig. 2, the estimated β is 0.51° (0.009 rad) and thus $x = 18$ nm, similar to previously reported values ranging from 10 to 20 nm for Activ[TM] glass [21,25].

3.3. Photodecolorization of AB9 and RBk5—thin multilayers

Degradation of AB9 and RBk5 is tracked by UV–vis spectroscopy, as shown in Fig. 3a and b, respectively. Photographs also are obtained (not included), revealing visual decolorization. Using the Prevo/Velev [24] deposition method, we are unable to achieve sub-monolayer coverage on the Activ[TM] glass because of its low surface area. To deposit sub-monolayer coverage, only 1 nmol dye can be deposited. For a 10 μL injection volume, this is about 0.1 mM dye solution. Such a small amount of dye is undetectable by UV–vis spectroscopy because it is masked by absorption from the glass substrate. Therefore, we used a uniform deposition of 2 mM dye corresponding to 40–45 monolayers of AB9 and 60–75 monolayers of RBk5 on the Activ[TM] glass, with a glass area ranging from 7.5 to 9.5 cm² and a dye area of $(1–2) \times 10^{10}$ cm²/ mol dye [27]. A monotonic decrease in absorbance is seen for AB9 ($\lambda_{max} = 629$ nm) and RBk5 ($\lambda_{max} = 597$ nm) as UV
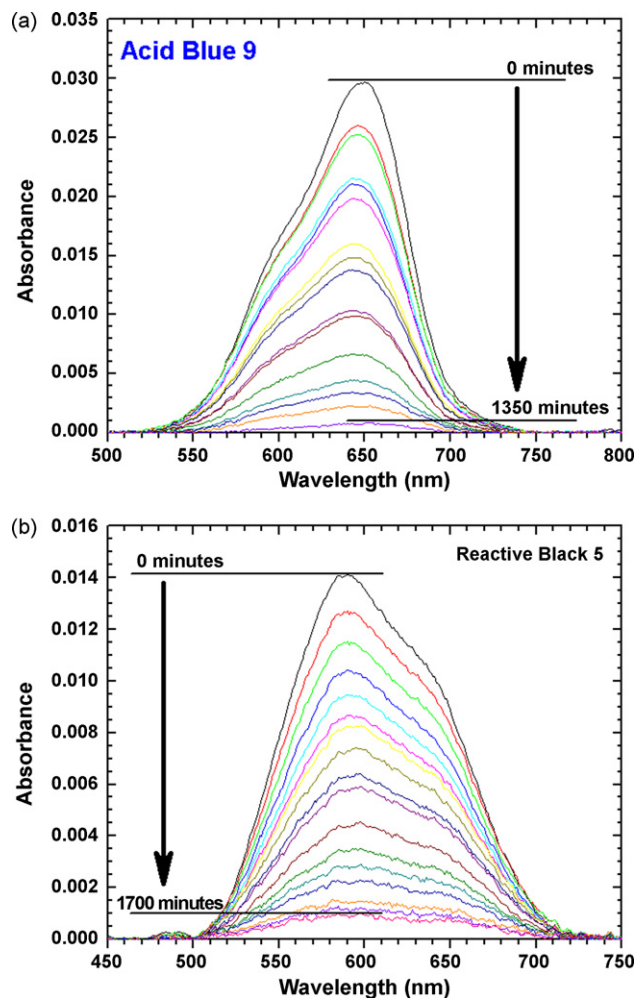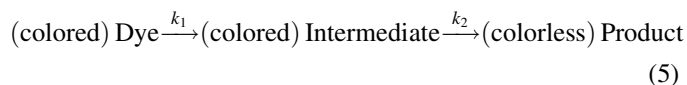
Fig. 3. Absorbance vs. wavelength as a function of time for dyes on Activ™ glass: (a) Acid Blue 9; (b) Reactive Black 5.

illumination time increases, which corresponds to dye decolorization.

3.4. Decolorization kinetics

A simple reaction mechanism for decolorization of AB9 and RBk5 sub-monolayer dry deposits on TiO_2 powders has been published previously [9], including a derivation of a time-dependent absorbance kinetic model for the two step, series reaction. Briefly, the simplified reaction involves colored dye conversion to a colored pseudo-intermediate compound continuing on to its colorless final product(s) (Eq. (5)):

$$(\text{colored})\ \text{Dye} \xrightarrow{k_1} (\text{colored})\ \text{Intermediate} \xrightarrow{k_2} (\text{colorless})\ \text{Product} \tag{5}$$

The total absorbance measured by UV–vis contains contributions from both dye and intermediate compounds. The absorbance kinetic model is shown in Eq. (6), where Abs_0 is the initial absorbance at 0 min, α_D and α_I are the dye and pseudo-intermediate molar absorptivities, respectively, k_1 is the first-order reaction rate constant from dye to intermediate (min^{-1}), k_2

is the first-order reaction rate constant from intermediate to product (min^{-1}), and t is the UV illumination time (min). The parameters k_1, k_2, and α_I/α_D are estimated using the asymptotic forms of Eq. (6) at short times where $t \to 0$ (Eq. (7)) and at long times (large t) (Eq. (8)). We assumed that $k_1 > k_2$ and that homogeneous photolytic effects are negligible [9]:

$$\text{Abs}(t) = \text{Abs}_0 \left\{ \left[\frac{\alpha_I}{\alpha_D} \frac{k_1}{k_2 - k_1} \right] [\exp(-k_1 t) - \exp(-k_2 t)] \right.$$
$$\left. + \exp(-k_1 t) \right\} \tag{6}$$

$$\frac{\text{Abs}(t)}{\text{Abs}_0} - 1 = k_1 t \left(\frac{\alpha_I}{\alpha_D} - 1 \right), \quad t \to 0 \tag{7}$$

$$\ln \left(\frac{\text{Abs}(t)}{\text{Abs}_0} \right) = \ln \left(-\frac{\alpha_I}{\alpha_D} \frac{k_1}{k_2 - k_1} \right) - k_2 t, \quad t \to \text{large} \tag{8}$$

The fit for the two step series reaction model using the asymptote analyses is shown in Fig. 4. The model fits the AB9 data (Fig. 4a) slightly better than the RBk5 data (Fig. 4b). A
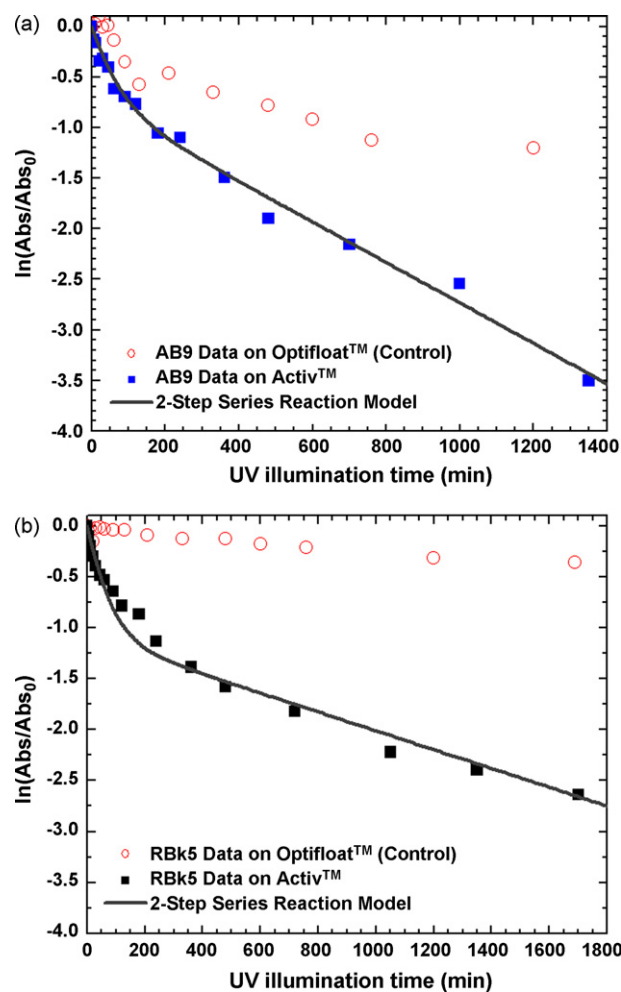

Fig. 4. ln(normalized absorbance) vs. time for dyes: (a) Acid Blue 9 and (b) Reactive Black 5. The squares represent data on Activ™ glass, the circles represent data on Optifloat™ glass (control), and the lines represent the two step series reaction model.

Table 2
Summary of kinetic parameters estimated from the two step series reaction model

Dye	Dye coverage type	Analysis type	k_1 (min^{-1})	k_2 (min^{-1})	α_I/α_D	Avg k_1 (min^{-1})	Avg k_2 (min^{-1})	Avg α_I/α_D
Reactive Black 5 (laboratory experiment)	Thin multilayer	Asymptote analysis	0.021	0.0015	0.46			
Reactive Black 5 (laboratory experiment)	Thin multilayer	LM algorithm	0.035	0.0021	0.56	0.028	0.0018	0.51
Acid Blue 9 (laboratory experiment)	Thin multilayer	Asymptote analysis	0.017	0.0020	0.51			
Acid Blue 9 (laboratory experiment)	Thin multilayer	LM algorithm	0.029	0.0026	0.62	0.023	0.0023	0.56
Acid Blue 9 (solar experiment)	Thin multilayer	Asymptote analysis	0.041	0.0057	0.74	–	–	–
Reactive Black 5 (laboratory experiment)	Thick multilayer	Asymptote analysis	0.0085	0.00012	0.65	–	–	–
Acid Blue 9 ([9] indirect analysis data)	Sub-monolayer coverage	Asymptote analysis	0.12	0.0021	0.56			
Acid Blue 9 ([9] direct analysis data)	Sub-monolayer coverage	Asymptote analysis	0.16	0.0007	0.15	0.14	0.0014	0.35
Reactive Black 5 ([9] indirect analysis data)	Sub-monolayer coverage	Asymptote analysis	0.12	0.0022	0.59			
Reactive Black 5 ([9] direct analysis data)	Sub-monolayer coverage	Asymptote analysis	0.14	0.0007	0.27	0.13	0.0014	0.43

summary of the kinetic parameters evaluated from Fig. 4 data (Table 2) shows that k_1 and k_2 values are similar for each dye, indicating an insensitivity to dye type. This behavior was also observed in our previous work with sub-monolayer deposits on TiO$_2$ powders [9]. Using all the data, the same kinetic parameters also are evaluated with the nonlinear curve fit function of Microcal Origin®. The function utilizes the Levenberg–Marquardt (LM) algorithm to determine the best fit, and requires Eq. (6) and initial parameter estimates as input, where the latter are those obtained from the asymptote analyses. The respective parameter values fitted over the entire data range using the LM algorithm are the same order of magnitude as found by the asymptote analyses (see rows 1–4 in Table 2).

To achieve 90% dye decolorization, or $\ln(\text{Abs}/\text{Abs}_0) \approx -2.5$ in Fig. 4, AB9 takes ~850 min versus ~1200 min for RBk5. Possible influences include: (a) RBk5 has a higher MW and thus higher carbon content compared to AB9 (Table 1); (b) the RBk5 disazo structure or its intermediate may be less reactive than the triphenylmethane framework in AB9 or its reaction intermediates. The latter possibility is supported by the fact that the pseudo-intermediate decolorization rate constant, k_2, is smaller for RBk5 than AB9 (Table 2).

Previous dye PCO work in our lab [9] for opaque (Abs $\geq$ 2) TiO$_2$ powder layers used the same absorbance kinetic model for sub-monolayer deposits of dyes AB9, RBk5, RB19, and AO7, and found an average k_1 and k_2 of 0.13 and 0.0014 min^{-1}, respectively, and a α_I/α_D of 0.56 for the indirect analysis data and 0.19 for the direct analysis data (Table 2). A comparison of the present dye multilayer results to previous sub-monolayer work revealed similar k_2 and α_I/α_D values, while an order of magnitude difference was seen in k_1. Three explanations are considered for the smaller k_1 on Activ^{TM} glass.

First, the TiO$_2$ preparation method and phases are different. The previous work [9] used Degussa P25 TiO$_2$ powder, a 70:30 mixture of anatase:rutile phases. The Activ^{TM} glass was coated by chemical vapor deposition of a SiO$_2$ blocking layer and then a TiO$_2$ layer formed from titanium chloride and ethyl acetate

precursors [25]. The Activ^{TM} TiO$_2$ layer is comprised solely of anatase phase. Previous literature cited an advantageous effect of mixing anatase and rutile on the reaction rate [28–30], but the mechanism was ambiguous. Bickley et al. [31] studied the Degussa P25 structure and postulated a synergistic effect of the thin rutile overlayer on the anatase particles, creating an increased efficiency in electron–hole separation by transferring valence band holes from anatase to rutile. Hurum et al. [32] used electron paramagnetic resonance spectroscopy (EPR) to hypothesize a conduction band electron transfer from rutile to a lower energy anatase lattice trapping site. Conversely, Datye et al. [33] reported no mixing of anatase and rutile phases in Degussa P25, and theorized that well-developed crystallinity in each phase resulted in a decrease in electron–hole recombination. Regardless of the mechanism, Ohno and coworkers found (a) a 3× higher acetone production rate from aqueous phase 2-propanol oxidation on Degussa P25 versus pure rutile [28], and (b) a 10× and 3× increase in liquid phase naphthalene oxidation on Degussa P25 versus pure anatase and pure rutile, respectively [29].

Second, the TiO$_2$ layer on the Activ^{TM} glass is very thin (10–20 nm) and does not absorb all incident UVA light. Peill and Hoffmann [34] calculated from the Beer–Lambert law that 2 and 5 μm thick TiO$_2$ layers coated on fiber-optic cables absorbed 45% and 95% of the refracted UV light, assuming a αC of 0.3 or 0.6 μm^{-1}, respectively. Julson and Ollis [9] stated that 5 μm was approximately 0.5% of the total TiO$_2$ powder layer thickness for their Direct Analysis data. Thus, about 100% UV light was absorbed in their TiO$_2$ layer. Mills et al. [21] estimated an absorbance of 0.065 (14%) at 365 nm for the TiO$_2$ layer on the Activ^{TM} glass. This corresponds to reduction in TiO$_2$ photon absorption from our previous work (100%) on opaque TiO$_2$ powders to our present work (14%) with Activ^{TM} glass. The number of photoexcitations and the rate of electron–hole separation per unit area diminish, leading to decreased reaction kinetics. If we normalize all k_1 values from the asymptote analyses to the calculated % UV light absorbed, then

our previous and present work collapse to the same ratio of $k_1/I_{abs} = 0.14$ min^{-1}/% photon absorbed.

Third, the dyes RBk5 and AB9 may absorb incident UV light (internal filter effect), decreasing the number of photons that reach the TiO$_2$ layer. Tang and Chen [35] postulated similar behavior for TiO$_2$ oxidation of aqueous RBk5 solutions in an annular photoreactor. They stated that higher RBk5 concentrations increased the solution opacity and reduced the number of incident photons that reached the TiO$_2$ surface, leading to a decrease in TiO$_2$ electron photoexcitation. Julson and Ollis [9] applied a sub-monolayer dye coverage, and noted that the dyes did not absorb photons appreciably. In contrast, the present work has coated 40–75 monolayers of dye, potentially decreasing the incident UVA and thus the TiO$_2$ photon absorption rate. Standard solutions were tested for dye absorption in the UV range. Reactive Black 5 has a maximum at $\lambda_{max} = 392$ nm with a molar absorptivity $\alpha_{RBk5, \, 392 \, nm} \approx 2830$ L/(mol cm) (2.83×10^6 cm^2/mol), while Acid Blue 9 peaks at $\lambda_{max} = 408$ nm with $\alpha_{AB9, \, 408 \, nm} \approx 8730$ L/(mol cm) (8.73×10^6 cm^2/mol). From the molarity and injected volume of the dye solution, and the Activ^{TM} area covered by the dye, we estimate C_{app} as $(3–4) \times 10^{-9}$ mol/cm^2. The corresponding dye absorbance of UV light is calculated from the Beer–Lambert law, with a maximum of 3–6% UVA absorption. This effect is likely the least important among the three proposed, because α is not too large in the UVA range, and our dyes form only thin multilayers for all but one case in Table 2.

In conclusion, the primary difference between our current and previous work is the % UVA absorption. Normalization of our rate constants to the variable % light absorption leads to nearly identical rate constant k_1 for the prior sub-monolayer and current multilayer experiments.

Control experiments on the dye-coated Optifloat^{TM} glass, shown as circles in Fig. 4a and b, reveal an unexpected decolorization of both dyes. Previous work by Julson and Ollis [9] using the same photoreactor as our experiments observed negligible homogeneous photodegradation of a sub-monolayer coverage of the same dyes, AB9 and RBk5, on Al$_2$O$_3$ powder, a photo-inert support, under 480 min of 1.3 mW/cm^2 UV light illumination. In contrast, there is 50% and 15% AB9 and RBk5 decolorization, respectively, after 480 min of UV irradiance on the Pilkington Optifloat^{TM} glass, leading us to assume there may be a photoactive material in the float glass. Semiconductor oxides, such as Fe$_2$O$_3$ and SnO$_2$, can be added to float glass for color/tint. Miyauchi et al. [36] reported methylene blue dye degradation on SnO$_2$ thin films under 100 min of 2 mW/cm^2 UVA irradiance. Though Miyauchi et al. [36] stated that Fe$_2$O$_3$ is photo-inactive for methylene blue degradation up to 100 min, their figure showed a slight decrease in absorbance. It is possible that appreciable dye degradation on Fe$_2$O$_3$ can occur over a period of 2000 min UV illumination. Given our results and the previous literature, we hypothesize the float glass may be photoactive, but not to the extent of the TiO$_2$-coated Activ^{TM} glass. Further studies on float glass will be conducted in our lab to clarify this effect.

Mills et al. [21] and Sanderson and Knowles [25] state that with Activ^{TM} glass, a 25–40 nm thick silicon oxide, presumably

SiO$_2$, blocking layer exists between the float glass and the TiO$_2$ thin film. This blocking layer prevents metal migration from the float glass to the TiO$_2$ layer. Therefore, we assume there is no other photoactive material on the surface of the Activ^{TM} glass except TiO$_2$, and the multilayer dye decolorization kinetics measured in Fig. 4a and b are solely for PCO by TiO$_2$.

3.5. Solar experiments

Solar tests to decolorize AB9 were conducted outdoors; example results are shown in Fig. 5. For a uniform deposition of 2 mM AB9, there are 55 monolayers on the Activ^{TM} glass. The AB9 achieves 95% decolorization in 480 min of solar UV illumination. These results are faster than the indoor laboratory experiments, which take about 850 min to achieve 90% AB9 decolorization. The number of incident photons is estimated for indoor and outdoor experiments by assuming 1 mW/cm^2 corresponds to $\sim 1.8 \times 10^{15}$ photons/(cm^2 s) for a emission wavelength of 365 nm, as calculated using the Planck relation and the wave theory of light [37]:

$$E = h\nu = \frac{hc}{\lambda} \tag{9}$$

$$\frac{\text{mol photons}}{\text{cm}^2 \, \text{s}} = \frac{E / (\text{cm}^2 \, \text{s})}{(hc/\lambda)/N_A} = \frac{I}{(hc/\lambda)/N_A} \tag{10}$$
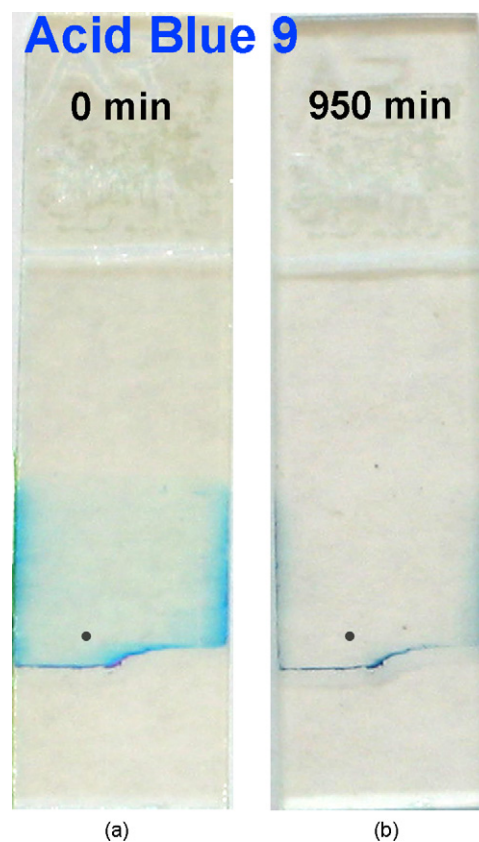

Fig. 5. Solar experiments demonstrating visual decolorization of Acid Blue 9 on Activ^{TM} glass from (a) 0 min to (b) 950 min. The grey dots represent the approximate location sampled by UV–vis absorbance measurements.

where E is the total incident photon energy (J), I the UVA irradiance (mW/cm^2), h the Planck's constant (6.63×10^{-34} J s/photon), c the speed of light in vacuum (2.998×10^8 m/s), λ the wavelength (nm), and N_A is the Avogadro's number (6.023×10^{23} photons/mol). The number of UVA incident photons reaching the Activ^{TM} surface is similar for 480 min of exposure, regardless if tested in the controlled laboratory photoreactor with 1.23×10^{-4} mol photons/cm^2 (1.4 mW/cm^2 irradiance) or 1.47×10^{-4} mol photons/cm^2 in the solar experiments (time-weighted value because of variable irradiance). Though total UVA exposure was similar in both cases, the solar experiments decolorized faster. This may be partly accounted for by sunlight UVB photons which also photoexcite TiO$_2$, while the laboratory photoreactor emits only UVA photons in the 315–400 nm range. About 4% of ground level UV light is dermatological UVB (dUVB, 290–320 nm) while dermatological UVA (dUVA, 320–400 nm) makes up the remaining 96% [38].

Additionally, the temperature and humidity are slightly higher outdoors. The TiO$_2$ reaction rate is roughly temperature independent, though electron–hole recombination may rise with increasing temperature. Obee and Brown [39] saw a mixed positive/negative temperature effect on oxidation rates under partial mass transfer influence: for gaseous toluene and 1,3-butadiene, oxidation rates increased when the temperature rose from ∼24 to ∼60 °C, while formaldehyde oxidation rates decreased under similar conditions. Humidity has two influences on the reaction rate [39,40]. At minimal water concentrations, higher humidity increases the reaction rate because of increased OH$^\bullet$ production. For some compounds, excessive humidity decreases the reaction rate because water displaces weakly adsorbed pollutants (e.g., aldehydes, aromatics), inhibiting the reaction. This effect was observed by Peral and Ollis [40] for *m*-xylene destruction and for oxidation of toluene, 1,3-butadiene, and formaldehyde by Obee and Brown [39]. Even though indoor and outdoor experiments exhibited similar water vapor densities of 6.4 g/m^3 (8000 ppmv at STP, 28% relative humidity at 25 °C), the outdoor humidity fluctuated more. At 8000 ppmv, Obee and Brown [39] observed a small negative slope for trace level contaminants, i.e., < 3 ppmv, but at higher concentrations, i.e., 8 ppmv toluene, they saw a monotonic positive slope upon changing the humidity from 0 to 20,000 ppmv. Thus, a slight humidity effect, in combination with ground level UVB light, may explain why our solar experiments decolorized AB9 somewhat quicker than the indoor experiments.

The AB9 solar experiments involved variable UV irradiance, so we expected the model (Eq. (6)) to fit the data less well. Nonetheless, the solar absorbance data fit well to the two step series reaction model; the calculated k_1 and k_2 standard deviations are an order of magnitude smaller than their values. These AB9 kinetic parameters are shown in Table 2, where k_1 and k_2 for the solar tests are roughly double the laboratory photoreactor tests.

3.6. Effect of light intensity

Experiments were carried out to demonstrate the effect of light intensity on the reaction rate in our dye multilayer films.

Egerton and King [41] studied the intensity influence on TiO$_2$ PCO of liquid isopropanol to acetone. At weak light supply rates (less than 5×10^{15} quanta/s), there was a linear relationship between light intensity and reaction rate. At strong light supply rates (greater than 5×10^{15} quanta/s), the reaction rate varied with the square root of the light intensity, and electron–hole recombination was suggested to be the dominant process. Their work and later analyses by Turchi and Ollis [5] have become the basis for a power-law light intensity explanation of photocatalyzed kinetics, where I is the UV light intensity and p is the power-law dependency:

$$r_{\text{initial}} \propto I^p \begin{cases} \text{weak light intensity } (p = 1) \\ \text{medium light intensity } (0.5 \leq p \leq 1) \\ \text{strong light intensity } (p = 0.5) \end{cases} \quad (11)$$

Eq. (11) contains a transition regime in between the two asymptotic values of $p = 0.5$ and 1. Peral and Ollis [40] determined $p = 0.7$ for acetone vapor phase oxidation with a UV irradiance ranging from 3×10^{15} to 40×10^{15} photons/(cm^2 s). Mills and Wang [42] degraded aqueous 2-chlorophenol using Degussa P25 TiO$_2$ dispersions and thin films with a UVA irradiance of $(0.5$–$6.4) \times 10^{15}$ photons/(cm^2 s). They reported $p = 0.64$ for a TiO$_2$ dispersion and $p \approx 1$ for a TiO$_2$ thin film. They argued that TiO$_2$ thin films, under identical reaction conditions to their dispersions, were subject to lower light intensities because aggregate TiO$_2$ particles of about 0.44 μm diameter partially screened UV light from the smaller, photoactive TiO$_2$ particles in direct contact with the solution. Their TiO$_2$ thin films were coated on the reaction vessel inner wall, and since the UVA lamps enclosed the reactor, the TiO$_2$ films were irradiated from the back.

For our uniform dye deposition of 2 mM AB9, there are 35–45 monolayers on the Activ^{TM} glass. The UV light intensity ranges from 0.08 to 1.9 mW/cm^2, and we neglect intermediates by using only initial times (0–10 min). The series rate expression simplifies to a first-order irreversible reaction: $-r_{\text{initial}} = k_{\text{app},0} C_0$, where $k_{\text{app},0}$ is the apparent rate constant (min^{-1}) and C_0 is the initial dye concentration (mol/L). The intensity variation results are shown in Fig. 6a, where the three data points are best fit to Eq. (11) with $p = 0.44$ and a standard error of 0.02. This is close to the asymptotic regime of strong UV light intensity, which is unexpected.

Mills and Wang [42] stated that for TiO$_2$ dispersions, the transition regime for Degussa P25 was ∼$(2$–$3) \times 10^{15}$ *ultra*-band gap photons/(cm^2 s). The number of incident photons approaching the Activ^{TM} surface in the present work is listed in Table 3. Our values of 1.4×10^{15} and 3.5×10^{15} photons/(cm^2 s) are similar those estimated by Mills and Wang [42] for the transition regime, while 0.17×10^{15} photons/(cm^2 s) is below their transition regime. The Activ^{TM} glass follows their dispersion data because our TiO$_2$ particle diameters are small (less than 0.1 μm). Mills and Wang [42] estimated their thin film TiO$_2$ particle diameters to be ∼0.44 μm, four times larger than the Activ^{TM} TiO$_2$ particles.

Ching et al. [43] presented an empirical correlation for the effect of UV light intensity on the gas phase formaldehyde

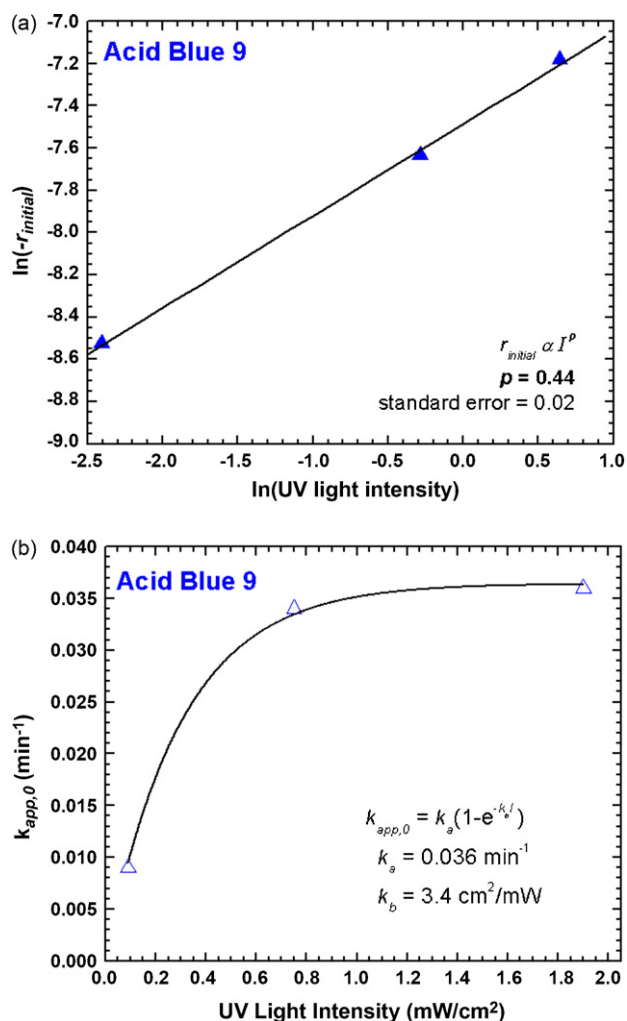Fig. 6. The effect of UV light intensity on reaction rates for Acid Blue 9 decolorization on Activ[TM] glass: (a) ln(initial reaction rate) vs. ln(UV light intensity); (b) $k_{app,0}$ as a function of UV light intensity.

Our values differed considerably from those reported by Ching et al. [43] for formaldehyde oxidation (k_a = 0.408 min^{-1}; k_b = 0.383 cm^2/mW), even though their calculated 13.6% UVA absorption plus scattering on sol–gel TiO$_2$ is similar to our 14% absorption on the Activ[TM] glass at 365 nm:

$$\frac{C}{C_0} = \exp[-k_{app,0}t] = \exp[-k_a t(1 - e^{-k_b I})], \quad k_{app,0}$$

$$= k_a(1 - e^{-k_b I}) \tag{12}$$

3.7. Photodecolorization of AB9 and RBk5—thick multilayers

Thick dye multilayers were uniformly deposited on the Activ[TM] glass using 10 mM solutions of RBk5 and AB9, corresponding to 260 and 150 monolayers, respectively. The linear motor was set to 4 mL/h (8.48 μm/s) and run at ambient lab air conditions (T = 25 °C, RH = 33%). Fig. 7 shows the decolorization of RBk5 thick multilayers on Activ[TM] glass. Similar results are seen on the AB9 dye. The absorbance peak for the thick multilayers in Fig. 7a is 4–5× greater than the thin multilayers in Fig. 3b, consistent with the mass loading increase, and the time needed for 90% decolorization is 10× greater on the thick multilayers (i.e., ~1050 min versus ~10,800 min). Thus, the % decolorization kinetics are slower on thick multilayers, shown in Fig. 7b, with k_1 = 0.0085 min^{-1}, k_2 = 0.00012 min^{-1}, and α_I/α_D = 0.65 (Table 2). Vinodgopal et al. [7] observed faster AO7 photosensitized degradation at low coverage (0.02 mmol AO7/g TiO$_2$) than at high coverage (0.10 mmol AO7/g TiO$_2$), attributed to a larger ratio of photon dose-to-dye molecules. Three explanations for the slower kinetics observed in thicker layers are considered.

First, RBk5 and AB9 will absorb more incident UV light which decreases the number of photons reaching the TiO$_2$ layer, as discussed in the third explanation of the decolorization kinetics section. We estimate that a maximum of 9% and 20% UVA (or approaching UVA) light is absorbed by RBk5 and AB9, respectively. As time progresses, the dye layer decreases and more photons reach the TiO$_2$ film.

Second, one intermediate may inadequately describe the system. There are certainly multiple intermediates in the true reaction mechanism. We extended our series kinetic model (Eq. (6)) to two intermediate compounds, with additional k_3 and α_{I2} series terms. Using the LM algorithm of Microcal Origin®,

oxidation rate for a transparent sol–gel TiO$_2$ thin film deposited on glass tubes. Using UVA irradiances ranging from 0 to 1.6 mW/cm^2, they suggested Eq. (12) where $k_{app,0}$ was the apparent rate constant (min^{-1}) and k_a (min^{-1}) and k_b (cm^2/mW) accounted for the effects of UV exposure time t (min) and UV irradiance I (mW/cm^2), respectively. We applied Eq. (12) to the LM algorithm of Microcal Origin® using our intensity influenced kinetic data for dyes, finding the best fit k_a and k_b values of 0.036 min^{-1} and 3.4 cm^2/mW, respectively (Fig. 6b).

Table 3
Summary of the variable UV light intensity parameters reported in the present work and previous literature

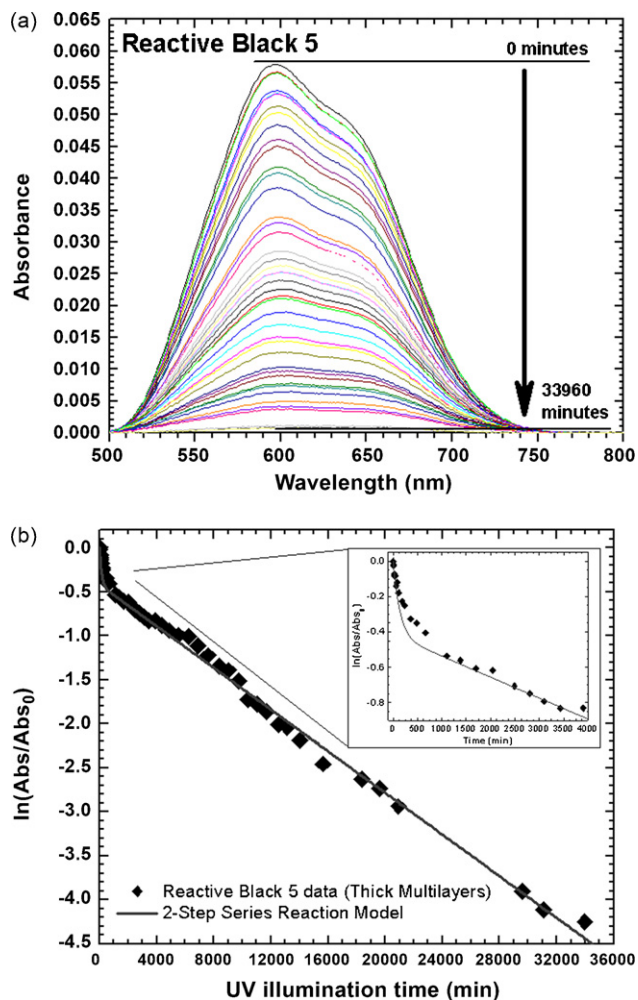| Reference	Irradiated area (cm^2)	UV light intensity		UV supply rate (photons/(cm^2 s))
		mW/cm^2	Photons/(cm^2 s)	
This work	11.3	0.09	0.17 × 10^{15}	1.9 × 10^{15}
	9.45	0.75	1.4 × 10^{15}	13 × 10^{15}
	10.4	1.9	3.5 × 10^{15}	36 × 10^{15}
Egerton and King [41]	–	–	–	10^{13} to 10^{19}
Mills and Wang [42]	120.5	–	(0.50–6.4) × 10^{15}	–
Peral and Ollis [40]	7.7	–	(3–40) × 10^{15}	–

Fig. 7. Decolorization plots of thick multilayers (260 monolayers) of Reactive Black 5: (a) absorbance vs. wavelength as a function of time; (b) ln(normalized absorbance) vs. time, where the points represent data and the line represents the model. The inset graph in (b) magnifies the 0–4000 min region.

we calculate $k_1 = 0.053$ min^{-1}, $k_2 = 0.0033$ min^{-1}, and $k_3 = 0.00012$ min^{-1}, with $\alpha_{I1}/\alpha_D = 0.92$ and $\alpha_{I2}/\alpha_D = 0.65$. These k_1 and k_2 values are the same order of magnitude as the thin multilayer values.

Third, inorganics in the original dye may accumulate and progressively deactivate TiO_2 sites. Both RBk5 and AB9 contain N, S, and Na. If these inorganics appear as nonvolatile products (e.g., NH_4^+, NO_3^-, SO_3^-, SO_4^{2-}, Na^+), they may build up and contribute to apparent deactivation.

A combination of these three effects should account for why the kinetic rate constants were slower for thick dye multilayers.

4. Conclusions

Pilkington Activ^{TM} glass was tested for decolorization of organic dye multilayer films of Reactive Black 5 and Acid Blue 9 in an air–solid system. Dye deposition on the glass was carried out by a horizontal coat method. Characterization of the Activ^{TM} glass using atomic force microscopy yielded a TiO_2 average particle diameter of 95 nm and an average thickness of 12 nm. X-ray diffraction results revealed only anatase phase

TiO_2. A TiO_2 crystallite thickness of 18 nm was estimated using the Scherrer equation.

Dye layer decolorization was observed visually and using UV–vis spectroscopy. A monotonic decrease in absorbance was seen with increasing UV illumination time. The kinetics for thin and thick dye multilayers were fitted to a two step series reaction model previously developed in our lab for dye sub-monolayers dried onto TiO_2 powders. In the simplified reaction scheme, the colored dye formed a colored intermediate before its colorless final product. The model fitted our multilayer data adequately for both RBk5 and AB9 using the asymptote analyses at $t \rightarrow 0$ and at long times (large t). The Levenberg–Marquardt algorithm was utilized to check the kinetic parameter values obtained from the asymptote analyses, and yielded new parameter values of the same order of magnitude as the asymptotic approach.

Solar experiments on the Activ^{TM} glass decolorized AB9 faster than the laboratory photoreactor experiments after 480 min of UV exposure. The number of incident photons reaching the Activ^{TM} surface was similar for both indoor and outdoor experiments. Our simple kinetic model fitted the solar data well even though the UV light intensity varied with time. We hypothesize that the additional UVB photons in the solar spectrum, and the higher water vapor density outdoors account for the solar versus blacklight-blue activity differences.

Light intensity-influenced laboratory experiments showed a $p = 0.44$ (± 0.02 standard error) power-law dependency of the initial decolorization rate on the UV light intensity. This indicated that the experiments occurred in the "strong" light intensity regime. The pseudo-first order initial rate constant also was fitted to a previous empirical equation incorporating the effects of illumination time and light intensity.

Acknowledgements

References

[1] Pilkington Glass plc, http://www.pilkington.com/international+products/activ/ (Accessed in 2006).
[2] Pittsburgh Plate and Glass (PPG), http://www.ppgsunclean.com/ (Accessed in 2006).
[3] Saint Gobain, http://www.saint-gobain-glass.com/bioclean/ (Accessed in 2006).
[4] A. Fujishima, T.N. Rao, D.A. Tryk, J. Photochem. Photobiol. C: Photochem. Rev. 1 (2000) 1.
[5] C.S. Turchi, D.F. Ollis, J. Catal. 122 (1990) 178.
[6] T. Zubkov, D. Stahl, T.L. Thompson, D. Panayotov, O. Diwald, J.T. Yates, J. Phys. Chem. B 109 (2005) 15454.
[7] K. Vinodgopal, D.E. Wynkoop, P.V. Kamat, Environ. Sci. Technol. 30 (1996) 1660.

 [8] T.C.K. Yang, S.F. Wang, S.H.Y. Tsai, S.Y. Lin, Appl. Catal. B: Environ. 30 (2001) 293.

 [9] A.J. Julson, D.F. Ollis, Appl. Catal. B: Environ. 65 (2006) 315.

[10] A.J. Julson, D.F. Ollis, Conference Proceedings from Ninth Photocatalytic and Advanced Oxidation Processes for Treatment of Air, Water, Soil and Surfaces, San Diego, CA, 2004.

[11] F. Shiraishi, S. Yamaguchi, Y. Ohbuchi, Chem. Eng. Sci. 58 (2003) 929.

[12] K. Doushita, T. Kawahara, J. Sol–Gel Sci. Technol. 22 (2001) 91.

[13] S. Sitkiewitz, A. Heller, N. J. Chem. 20 (1996) 233.

[14] V. Romeas, P. Pichat, C. Guillard, T. Chopin, C. Lehaut, N. J. Chem. 23 (1999) 365.

[15] E.J. Wolfrum, J. Huang, D.M. Blake, P.C. Maness, Z. Huang, J. Fiest, W.A. Jacoby, Environ. Sci. Technol. 36 (2002) 3412.

[16] Y. Paz, Z. Luo, L. Rabenberg, A. Heller, J. Mater. Res. 10 (1995) 2842.

[17] T.N. Obee, Environ. Sci. Technol. 30 (1996) 3578.

[18] J.T. Remillard, J.R. McBride, K.E. Nietering, A.R. Drews, X. Zhang, J. Phys. Chem. B 104 (2000) 4440.

[19] E. Stathatos, D. Tsiourvas, P. Lianos, Colloids Surf. A: Physicochem. Eng. Asp. 149 (1999) 49.

[20] T. Porada, R. Gade, Zeitschrift Fur Physikalische Chemie (Int. J. Res. Phys. Chem. Chem. Phys.) 210 (1999) 113.

[21] A. Mills, A. Lepre, N. Elliott, S. Bhopal, I.P. Parkin, S.A. O'Neill, J. Photochem. Photobiol. A: Chem. 160 (2003) 213.

[22] B.E. Warren, X-Ray Diffraction, Dover Publications, Inc., Mineola, NY, 1990.

[23] O. Carp, C.L. Huisman, A. Reller, Prog. Solid State Chem. 32 (2004) 33.

[24] B.G. Prevo, O.D. Velev, Langmuir 20 (2004) 2099.

[25] K.D. Sanderson, J.A. Knowles, United States Patent and Trademark Office, Application 10/497886 (2005). Publication US 2005/0252108 A1.

[26] Joint Committee on Powder Diffraction Standards, International Centre for Diffraction Data (JCPDS-ICDD), Powder Diffraction File, Swarthmore, PA, 1998.

[27] A.J. Julson, Photocatalytic Decolorization of Organic Dyes in Titanium Dioxide–Air Systems, Thesis, North Carolina State University, 2005.

[28] T. Ohno, K. Sarukawa, M. Matsumura, J. Phys. Chem. B 105 (2001) 2417.

[29] T. Ohno, K. Sarukawa, K. Tokieda, M. Matsumura, J. Catal. 203 (2001) 82.

[30] C.Y. Wu, Y.H. Yue, X.Y. Deng, W.M. Hua, Z. Gao, Catal. Today 93–95 (2004) 863.

[31] R.I. Bickley, T. Gonzalezcarreno, J.S. Lees, L. Palmisano, R.J.D. Tilley, J. Solid State Chem. 92 (1991) 178.

[32] D.C. Hurum, A.G. Agrios, K.A. Gray, T. Rajh, M.C. Thurnauer, J. Phys. Chem. B 107 (2003) 4545.

[33] A.K. Datye, G. Riegel, J.R. Bolton, M. Huang, M.R. Prairie, J. Solid State Chem. 115 (1995) 236.

[34] N.J. Peill, M.R. Hoffmann, Environ. Sci. Technol. 29 (1995) 2974.

[35] C. Tang, V. Chen, Water Res. 38 (2004) 2775.

[36] M. Miyauchi, A. Nakajima, T. Watanabe, K. Hashimoto, Chem. Mater. 14 (2002) 2812.

[37] N. Serpone, E. Pelizzetti (Eds.), Photocatalysis: Fundamentals and Applications, John Wiley & Sons, Inc., New York, NY, 1989.

[38] F.J. Christiaens, A. Chardon, A. Fourtanier, J.E. Frederick, Photochem. Photobiol. 81 (2005) 874.

[39] T.N. Obee, R.T. Brown, Environ. Sci. Technol. 29 (1995) 1223.

[40] J. Peral, D.F. Ollis, J. Catal. 136 (1992) 554.

[41] T.A. Egerton, C.J. King, J. Oil Colour Chemists Assoc. 62 (1979) 386.

[42] A. Mills, J.S. Wang, Zeitschrift Fur Physikalische Chemie (Int. J. Res. Phys. Chem. Chem. Phys.) 213 (1999) 49.

[43] W.H. Ching, M. Leung, D.Y.C. Leung, Solar Energy 77 (2004) 129.